JOURNAL OF MATERIALS SCIENCE 29 (1994) 6152–6158

Methodology for the determination of the interfacial properties of brittle matrix composites

E. LARA-CURZIO, M. K. FERBER
Metals and Ceramics Division, Oak Ridge National Laboratory, Oak Ridge, TN 37831, USA

The interfacial properties of a glass-ceramic matrix composite (SiC/CAS) were determined from single-fibre push-out tests using the interfacial test system. The coefficient of friction, μ, the residual clamping stress, σ_c, and fibre axial residual stress, σ_z, were extracted by fitting the experimental stress versus fibre-end displacement curves using the models of Hsueh, and Kerans and Parthasarathy. Using Hsueh's model, the intrinsic interfacial frictional stress ($\tau = \mu\sigma_c$) was found to be 11.1 $\pm$ 3.2 MPa, whereas by using Kerans–Parthasarathy's model it was found to be 8.2 $\pm$ 1.5 MPa. Comparisons between these models are included, together with a discussion of data analysis techniques.

Nomenclature

σ_z	Axial fibre residual stress (Pa)
σ^*	Effective clamping stress (Pa)
σ_c	Residual clamping stress (Pa)
σ_p	Poisson's effect-induced clamping stress (Pa)
σ_d^0	Debond stress in the absence of residual stresses (Pa)
σ_d	Experimental debond stress (Pa)
σ	Compressive applied stress (Pa)
τ	Interfacial shear stress (Pa)
u	Fibre-end displacement (m)
h	Debond length (m)
r	Fibre radius (m)
E_f	Fibre Young's modulus (Pa)
E_m	Matrix Young's modulus (Pa)
ν_f	Fibre Poisson's ratio (dimensionless)
ν_m	Matrix Poisson's ratio (dimensionless)
f	Fibre volume fraction (dimensionless)
k	Parameter (dimensionless)
D	Parameter (dimensionless)
μ	Interfacial coefficient of friction (dimensionless)
G_i	Interface toughness ($J\,m^{-2}$)
C_m	Load-train compliance ($m\,N^{-1}$)

1. Introduction

Because the strength and toughness of continuous fibre-reinforced ceramic composites (CFCCs) are significantly influenced by the forces acting at the fibre–matrix interface, substantial efforts have been concentrated in recent years towards the mechanical characterization of the interfaces in these materials. These efforts have included both the development of experimental methods to determine the interfacial shear strength, and the sliding resistance between fibre and matrix, and also the formulation of analyses to model these tests.

The experimental methods currently available for the mechanical characterization of composite interfaces can be grouped into two categories [1]: single-fibre tests that include push-in, push-out, pull-out and fragmentation, and multiple fibre tests such as ball-indentation, slice compression and bundle push-out tests. Although the single-fibre pull-out and fragmentation tests best reproduce the mechanics of the interface in CFCCs when these materials are loaded in tension, these tests require the preparation of special samples that may not represent the true behaviour of the composite. Furthermore, the fragmentation test may only be used with composites that have a transparent matrix.

As a consequence, single-fibre push-in and push-out tests have been the most widely used. In principle, these two tests are variations of the same test, which consists of subjecting a single fibre, with its axis perpendicular to a polished cross-section of the composite, to compressive loading using a small indentor. The differences between the two tests are the length of the promoted debonding and the magnitude of the applied forces. In the case of push-in tests, fibre–matrix debonding occurs over a small fraction of the embedded fibre length (Fig. 1a), whereas debonding is promoted along the entire embedded fibre length for the push-out test. In the latter case, protrusion of the fibre from the bottom side of the composite results (Fig. 1b).

As a result of the limited load capacity of the systems currently available to conduct push-in tests (Nanoindentor, Nano Instruments. Knoxville, TN 37830, USA), testing has been restricted to the evaluation of composites with a weak fibre–matrix bonding or composites reinforced with small-diameter fibres. The limited load capacity is a direct consequence of the requirement for applying and controlling very minute loads. However, this instrument meets a critical requirement for conducting tests with small-diameter fibres which consists in reproducibly positioning the indentor on to a fibre within 1 μm.

0022–2461

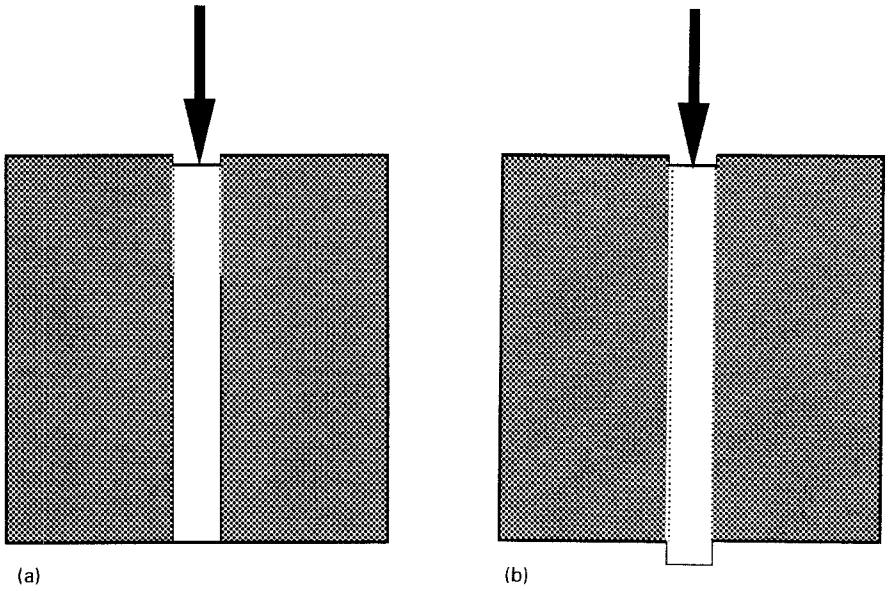

Figure 1 (a) Push-in test: fibre radius ≪ sliding length ≪ fibre embedded length. (b) Push-out test: sliding length ≈ fibre embedded length ≫ fibre radius.

Push-out tests, on the other hand, have been used exclusively for the characterization of composites reinforced with filaments or large diameter fibres (> 50 μm). Because the loads involved in this test are much larger than those for push-in tests, there is no need to measure or control them with a large degree of resolution. Also, positioning the indentor on to a large filament can easily be accomplished.

Recently, an interfacial test system (ITS) was designed and constructed at the Oak Ridge National Laboratory as part of the US Department of Energy CFCC program [2]. This apparatus was developed with the objective of filling in the gap between the capabilities of the Nanoindentor for push-in tests and existing apparatuses to conduct push-out tests [3, 4]. Some of the challenges in the design of this equipment were: (1) the ability to resolve the minute forces and displacements associated with push-in tests; (2) the load capability to conduct push-out tests in composites reinforced with either small- or large-diameter fibres, and (3) positioning reproducibly the indentor on to a selected fibre within 1 μm. A brief description of the ITS is presented in Section 2.1.2, but a more detailed presentation can be found elsewhere [2].

Parallel to the development of experimental methods and techniques to evaluate the interfacial properties of CFCCs, efforts have also been concentrated in the formulation of analyses to model these tests. In the absence of an exact elastic solution, a number of shear-lag [5–7], modified shear-lag [8] and finite-element analyses [9–13] have been presented to estimate the stress field around a fibre during push-in and push-out experiments.

Among the analytical models, those of Kerans and Parathasarathy (K–P) [6] and Hsueh [8] are the most amenable to use for analysing push-in and push-out experimental results (Other analyses have been presented since, and although different expressions have been derived for the stress versus fibre-end displacement relation, those models coincide in almost all respects with that of K–P, for example [7, 14].) Both of these models are applicable when progressive debonding and sliding occur during push-in or push-out, both consider the radial and axial residual stresses in the fibre, and assume a Coulomb frictional condition along the fibre–matrix interface. An additional feature of Hsueh's analysis is the provision for modelling the unloading process during push-in tests.

In this paper, the models of K–P and Hsueh are used to analyse the results of push-out tests of a SiC(Nicalon)/CAS composite (Corning Glass Works Corning, NY 14831). This composite was chosen because it has been widely used in the verification of micromechanical models in which the interfacial shear stress plays a major role. The value of the interfacial shear stress in this composite has been reported from direct measurements using indentation techniques [15, 16], bundle push-out tests [17], indirectly from measurements of the matrix cracking stress [18], from fibre pull-out distributions after tensile fracture [18], from crack spacing measurements [18], by fitting experimental σ–ε curves of unidirectional laminates using micromechanical models [19, 20] and from frictional heating experiments [21]. Table I summarizes these previously reported results.

TABLE I Summary of reported values for the interfacial shear stress of SiC/CAS

Technique	τ (MPa)
Indentation [15, 16]	10–19
Bundle push-out [17]	14–19
Matrix cracking stress [18]	10–15
Saturation crack spacing [18, 20]	9, 25–28
Mean fibre pull-out length [18]	10–15
Composite σ–ε behaviour [19, 20]	8–9
Frictional heating [21]	3.5–5
Single-fibre push-out (this work)	8.2–11.1

In the next section, the experimental procedure for push-out tests is described. The experimental stress versus fibre-end displacement push-out curves were then fitted with the models of K–P and Hsueh using the interfacial parameters μ, σ_c and σ_z as fitting parameters. The data analysis and discussion of the results and the fitting procedures are included.

2. Experimental procedure

2.1. The ITS

The operation of the interfacial test system is very similar to that of the Nanoindentor, except that the ITS operates under displacement control conditions and loading is accomplished by pushing the sample upwards into a fixed indentor (see Fig. 2). The test methodology consists of (1) selecting a fibre from the polished cross-section of the composite with the aid of a microscope and a video system, (2) translation of the sample underneath a flat-bottomed indentor, and (3) pushing the sample against a fixed indentor using a vertical translation stage. Different indentors (e.g. diamond or tungsten carbide) have been examined when testing composites containing fibres with diameters between 10 and 20 μm. For the tests reported here, a flat-bottomed 10 μm diameter diamond indentor was used. With the current apparatus, a fibre can be positioned underneath the indentor reproducibly within ± 1 μm in the X–Y plane. During the test, both the load and fibre-end displacement are recorded continuously with 1 mN and 0.1 μm resolution, respectively. Currently the load capacity of the system is limited only by the load capability of the Z-stage (13 kg).

The operation of the ITS is fully computerized and automated for data acquisition and control, and user intervention is only required to select the fibres that will be tested. A schematic description of the ITS system is presented in Fig. 2.

2.2. Sample preparation

A schematic illustration of the wedge-shaped sample geometry with typical dimensions is presented in Fig. 3. This geometry allows for the determination of the interfacial parameters (e.g. debond and push-out stresses) as a function of the fibre embedded length using only one sample.

To allow fibre protrusion from the bottom of the specimen during push-out, a thin layer of moulding clay is placed under the sample. The sample is then embedded in epoxy and polished using standard metallographic techniques, always insuring that enough material is removed during the polishing stage such that no damage remains from the cutting process.

3. Results

Fig. 4a and b show the raw and corrected stress versus fibre-end displacement curves from a typical push-out test with the ITS. In this case, the corrected curve was obtained by subtracting the contribution of the load-train deformation to the measured fibre-end displacement. The load-train compliance was determined from load versus displacement curves obtained by subjecting the sample to compression at various points along the wedge. To do so, the indentor was replaced with a 500 μm diameter stainless steel rod. Typical values for the compliance of the ITS and wedged CFCC samples, were between 4 and 6 μm N^{-1}. The corrected stress versus fibre-end displacement curves (Fig. 4b)

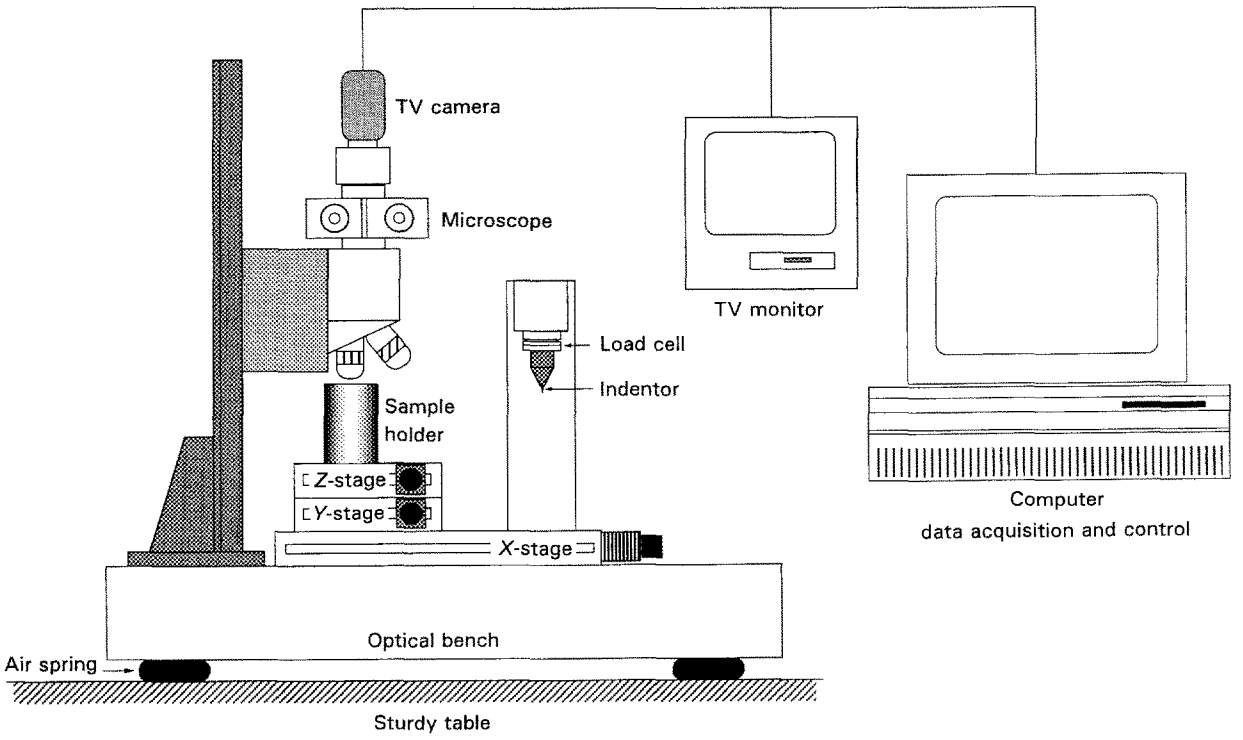

Figure 2 Schematic representation of the interfacial test system.

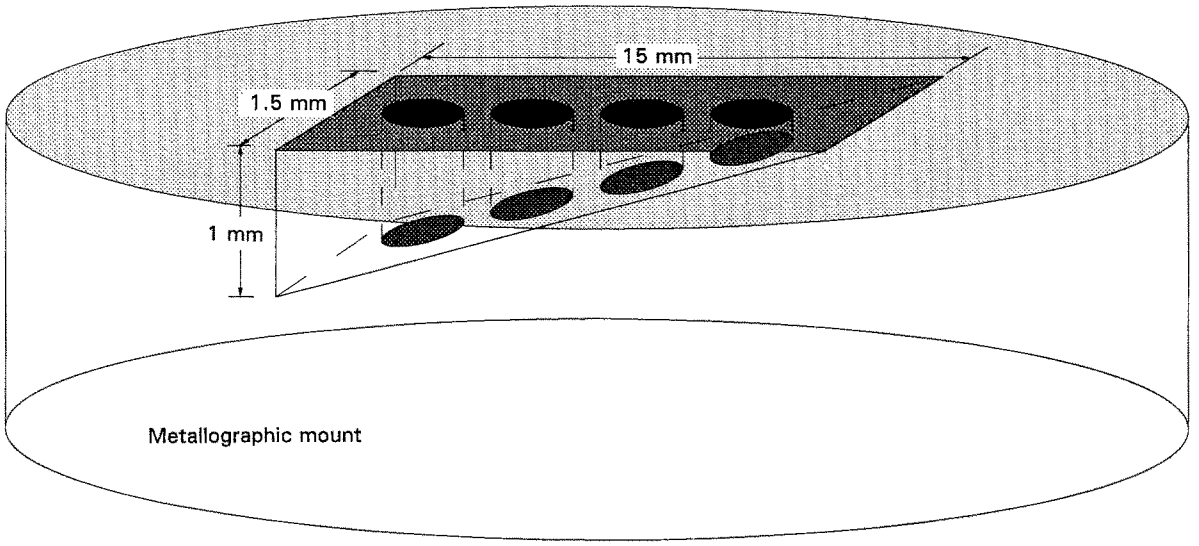

Figure 3 Wedge geometry for push-out test sample. Surface is prepared using conventional metallographic techniques.

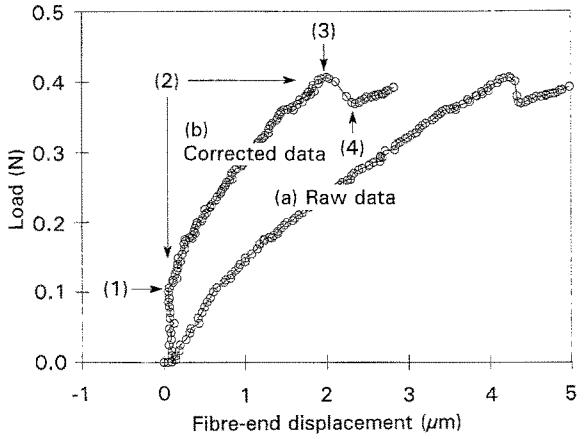

Figure 4 (a) Raw, and (b) corrected load versus fibre-end displacement curves. The corrected curve is obtained by subtracting the contribution from the deformation of the load train to the measured displacement. In curve (b), (1) corresponds to the initiation of debonding and sliding, (2) to the region of progressive debonding and sliding, (3) to the peak load, and (4) to the load drop that indicates that fibre push-out has occurred.

typically exhibited the following features: (1) initiation of debonding; (2) progressive debonding and sliding; (3) peak load, and (4) load drop after debonding was promoted along the entire embedded fibre length, resulting in fibre push-out.

4. Analysis

4.1. The model of Kerans and Parthasarathy

According to the model of Kerans and Parthasarathy [6], the rising part of the load–displacement curve during a single fibre push-out test is given by

$$u = \pi r^2 C_m \sigma + \frac{(1 - 2k\nu_f)r}{2\mu k E_f} \times \left[\sigma - \sigma_d^0 - \sigma_z + (\sigma^* - \sigma_d^0) \times \ln\left(\frac{\sigma^* - \sigma}{\sigma^* - \sigma_d^0 - \sigma_z}\right)\right] \quad (1)$$

where u is the measured fibre-end displacement for the applied stress σ, σ_z is fibre axial residual stress, C_m is the compliance of the load train and

$$k = \frac{E_m \nu_f}{E_f(1 + \nu_m) + E_m(1 - \nu_f)} \quad (2)$$

$$\sigma_d^0 = \left[\frac{4G_i E_f}{(1 - 2k\nu_f)r}\right]^{1/2} \quad (3)$$

$$\sigma^* = -\frac{\sigma_c}{k} \quad (4)$$

E_f, E_m, ν_f, ν_m are the Young's moduli and Poisson's ratios for the fibre and the matrix respectively, G_i is the mode II fracture toughness of the fibre–matrix interface and σ_d^0 is the stress required for debonding a fibre in the absence of residual stresses. Equation 1 is applicable when

$$\sigma_d = \sigma_d^0 + \sigma_z \leq \sigma \leq \sigma_{\text{push-out}} \quad (5)$$

where σ_d is the experimental value of the stress required to initiate debonding and sliding and $\sigma_{\text{push-out}}$ is the peak stress.

4.2. Hsueh's model

Hsueh has shown that by averaging the interfacial shear stress and Poisson's effect along the sliding length, the predictions are surprisingly accurate when compared to those from the complete analysis [24]. Based on these observations, a simplified version of Hsueh's original model has been considered here.

The fibre-end displacement predicted by Hsueh's model (after subtracting the contribution of the load-train deformation) for the applied stress, σ, is given by

$$u = \frac{h(\sigma + \sigma_d - 2\sigma_z)}{2E_f} \quad (6)$$

where σ_d is the experimental value of the stress required to initiate debonding and sliding and h is the sliding length. The sliding length and the interfacial

shear stress will be given by

$$h = \frac{r(\sigma_d - \sigma)}{2\tau} \quad (7)$$

$$\tau = -\mu(\sigma_c + \sigma_p) \quad (8)$$

where σ_p is the average contribution to the clamping stress due to Poisson's effect and is given as

$$\sigma_p = \left[\left(\frac{\nu_f E_m}{E_f} - \frac{f\nu_m}{1-f}\right)\sigma + \left(\frac{\nu_f E_m}{E_f} - \frac{f\nu_m}{1-f}\right)\sigma_d\right] \Big/ 2D \quad (9)$$

with

$$D = \frac{1+f}{1-f} + \nu_m + \frac{(1-\nu_f)E_m}{E_f} \quad (10)$$

Equation 6 is applicable when

$$\sigma_d \leq \sigma \leq \sigma_{\text{push-out}} \quad (11)$$

As indicated by Equation 7, there are two sources of the radial compressive stress at the fibre–matrix interface: (1) the residual clamping stress σ_c, which results from the thermoelastic mismatch between fibres and matrix, and (2) the stress σ_p, due to the fibre Poisson's expansion when subjected to an axial compressive stress. Because σ_p is a function of the axial stress in the fibre, it varies along the fibre length. Therefore, both the resultant radial stress at the fibre–matrix interface and the interfacial shear stress are non-uniform along the embedded length of the fibre.

5. Evaluation of interfacial properties

To determine the interfacial parameters, the experimental load versus fibre-end displacement curves were fitted with the models using μ, σ_c and σ_z as fitting parameters. Although, in principle, this is a simple proposition, in practice it is difficult to automate efficiently the fitting algorithm.

In general, the determination of the fitting parameters corresponds to the solution of an optimization problem, which can be formulated in terms of fulfilling the least squares criterion, i.e. the sum of the squared residuals (SOS) must be a minimum, or

$$\sum_{i=1}^{n} (u_i^* - u_i)^2 \equiv \text{minimum} \quad (12)$$

where u_i^* is the fibre-end displacement predicted by the regression model and u_i is the measured fibre–end displacement. To minimize the SOS, it is necessary that the following relations be met

$$\partial\left[\sum_{i=1}^{n} (u_i^* - u_i)^2\right] \Big/ \partial\mu = 0 \quad (13)$$

$$\partial\left[\sum_{i=1}^{n} (u_i^* - u_i)^2\right] \Big/ \partial\sigma_c = 0 \quad (14)$$

$$\partial\left[\sum_{i=1}^{n} (u_i^* - u_i)^2\right] \Big/ \partial\sigma_z = 0 \quad (15)$$

Although there is still considerable discussion with regard to the validity of the assumptions leading to Equation 3 [25, 26], this equation provides a relationship between the debond stress, σ_d, and the interface toughness, G_i. Therefore, because the value of σ_d ($\sigma_d = \sigma_d^0 + \sigma_z$) is readily available from the experimental stress versus fibre-end displacement curve, a unique relation can be established between G_i and σ_z, for example, in order to use Equation 15.

Because Equations 13–15 are non-linear, it is necessary to use iterative methods to find their solution. In the absence of efficient iterative procedures for systems of non-linear simultaneous equations [27] it is necessary to transform and simplify the original problem. For example, by combining Equations 13–15, a new function g is defined as

$$g = (f_1^2 + f_2^2 + f_3^2) \quad (16)$$

where f_1, f_2 and f_3 are the functions in Equations 13–15, respectively. The new function is positive everywhere, except at the solution of the set of Equations 13–15 where it is identically zero. Therefore, the problem of finding a solution to three simultaneous equations is reduced to finding the solution of a single equation. Another property of this new function g, is that its solution coincides with a minimum. Therefore, to find its solution, we just have to follow the gradient of g downhill (The gradient of g points toward the opposite direction to the minimum.)

However, given the nature of the stress versus fibre-end displacement relations, the efficient automation of the algorithm outlined above is difficult. Because a large number of combinations of μ and σ_c give the same value of τ, that in turn produces very similar stress versus fibre-end displacement curves, the space defined by μ–σ_c–σ_z–SOS, and consequently that defined by μ–σ_c–σ_z–g will be filled with local minima. Fig. 5a illustrates the described condition with a plot of the μ–σ_c–SOS space for a constant value of σ_z. Fig. 5b is a magnified view of the bottom valley of Fig. 5a. The existence of a large number of local minima prevents the insurance that the absolute minimum will always be reached at the end of the iterative process, because the trajectory of the search will be controlled by the strongest attractor, which does not necessarily correspond to the absolute minimum [28].

An alternative solution to the problem of finding the absolute minimum in the μ–σ_c–σ_z–SOS space consists in mapping the entire space using a fine mesh within a wide boundary. Although this approach is not elegant, it is very efficient and guarantees that the absolute minimum will always be found. This is the approach that we have chosen to adopt.

In the process of mapping the μ–σ_c–σ_z–SOS space, computations are carried out only if the following condition is met

$$\text{thickness} - nr < \text{debond length} < \text{thickness} \quad (17)$$

where n is unknown, although recently it was suggested from numerical analyses that $n = 1.5$ [7]. However, without losing generality, we have used a value of $n = 4$ during the data analysis. When the debond length equals thickness $- nr$, the crack along the

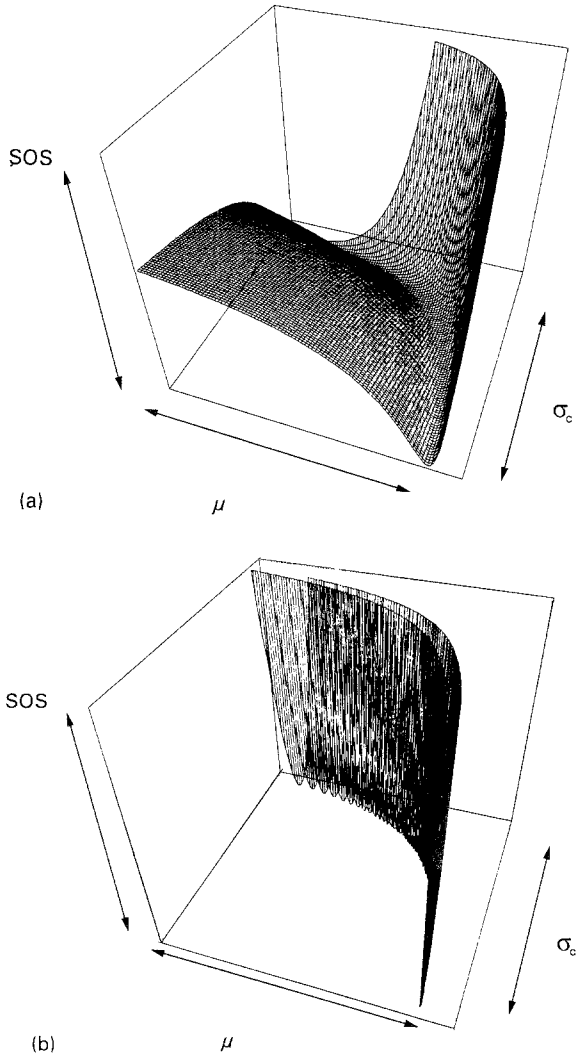

Figure 5 (a) Map of the μ–σ_c–SOS for constant σ_z. (b) Magnified view of the bottom valley of the surface in (a). These maps illustrate the difficulties in using automated iteration functional procedures to determine the absolute minimum in a space filled with local minima.

fibre–matrix interface becomes unstable and propagates catastrophically. This results in the load drop observed at push-out, as the system releases part of the stored energy to debond the remaining portion of bonded interface (point 3, Fig. 4b).

Using the following elastic constants $E_f = 200$ GPa, $E_m = 80$ GPa, $\nu_f = 0.2$, $\nu_m = 0.3$, the results of fitting ten experimental stress versus fibre-end displacement push-out curves using the models of K–P and Hsueh are presented in Table II. Table II includes values for the coefficient of friction, the residual clamping stress and the fibre axial stress, while Fig. 6 shows an experimental stress versus fibre-end displacement curve, along with the predictions of K–P and Hsueh models indicating the goodness of the fit.

TABLE II Interfacial properties for SiC/CAS composite according to the predictions of Hsueh and K–P models for push-out tests

	μ	σ_c (MPa)	σ_z (MPa)
K–P analysis	0.05 ± 0.03	-240 ± 175	-152 ± 114
Hsueh analysis	0.06 ± 0.02	-195 ± 74	-141 ± 121

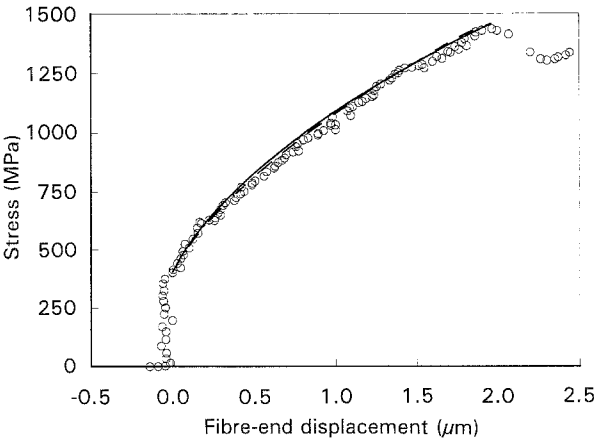

Figure 6 Comparison of the predictions of (——) Hsueh and (– – – –) Kerans–Parthasarathy models along with experimental push-out curves for SiC/CAS composite.

6. Discussion

The values obtained for the intrinsic interfacial frictional stress ($\tau = \mu\sigma_c$) on a test basis using K–P's analysis (8.2 ± 1.5 MPa), are slightly lower than those obtained when using Hsueh's analysis (11.1 ± 3.2). However, the product of the average values for the coefficient of friction and the clamping stress according to the K–P analysis predictions (12.0 MPa) agrees well with that obtained when using Hsueh's analysis (11.7 MPa). The large scatter, as inferred from the standard deviations is another manifestation of the observation made in the last section, i.e. that different combinations of μ and σ_c would yield the same value of τ and therefore similar stress versus fibre-end displacement curves.

The value for τ obtained in this study is in fair agreement with other measurements involving indentation techniques [15, 16] and from bundle push-out tests [16]. Although the bundle push-out test may be desirable to average the inherent variations between single-fibre tests, this test is restricted to those composites where the matrix can be etched away without damaging the fibres.

The value obtained for τ in this study is also in agreement with values inferred to fit tensile σ–ε curves of unidirectional composites and to predict their unloading uniaxial modulus, both using micromechanical models [18]. Large disagreement was found however, with the value obtained for the interfacial shear stress from crack spacing measurements (25–28 MPa) [18], and it is likely that these differences result from the underlying assumptions in the micromechanical models used in those studies. Although the results obtained in this study for the interfacial shear stress cannot be compared directly to those obtained from frictional heating experiments, it is worth noticing that the value of 3–5 MPa obtained for the dynamic shear stress from frictional heating experiments [21], is consistent with the fact that the magnitude of the interfacial shear stress will decrease as wear damage accumulates at the fibre–matrix interface during fatigue.

The value predicted for the clamping stress using both the Hsueh and K–P models, is larger than that

expected from the pure thermoelastic mismatch between the fibres and the matrix (−65 MPa [18]). This suggests, not surprisingly, that the effect of asperities and roughness of the fibre surface, and non-uniform fibre diameters, may influence the frictional characteristics of the interface. Although both of these models in their current form combine all these effects into σ_c, it may be possible to separate these effects by introducing a constant component of the interfacial shear stress, τ_0

$$\tau = \tau_0 + \mu(\sigma_c + \sigma_p) \quad (18)$$

which is independent of the clamping stress at the interface due to residual stresses, and that arises from the roughness of the fibre surface [7, 14].

Furthermore, although it is always intended to minimize any effects of the sample preparation procedures in the state of the residual stresses of the composite, the distribution of residual stresses in the sample is undoubtedly very complex, particularly for the axial stress in the fibre. Therefore, a large scatter in the predicted values of the fibre axial residual stress should be expected (and for G_i, when using K–P's analysis). The expected value for the axial residual stress in the fibres is −89 MPa [18].

7. Conclusions

The interfacial properties of a SiC/CAS unidirectional composite were determined from single-fibre push-out tests using the interfacial test system. The interfacial parameters μ, σ_c and σ_z were determined by fitting the experimental stress versus fibre-end displacement curves using the models of Kerans–Parthasarathy and Hsueh. In the absence of efficient functional iteration routines to solve the optimization equations from the fitting problem, the interfacial parameters were obtained by mapping out the μ–σ_c–σ_z–SOS space to determine the combination of μ–σ_c–σ_z that provides the smallest sum of squares.

Typical values between 0.05 and 0.06 were obtained for the coefficient of friction and between −195 and −240 MPa for the clamping stress. The resulting interfacial shear stress (8–12 MPa) is in good agreement with published results from other indentation techniques, from bundle push-out tests, and with those inferred by fitting experimental σ–ε tensile test curves of unidirectional laminates using micromechanical models. Although large scatter was observed for the axial fibre residual stress predicted by these models, the actual state of residual stresses existing in a single fibre is particularly complex and may not be fully represented by the underlying assumptions in the models considered.

Acknowledgements

This work was sponsored by the US Department of Energy, Assistant Secretary for Conservation of Renewable Energy, Office of Industrial Technologies, Industrial Energy Efficiency Division, under contract DE-AC05-840R21400 with Martin Marietta Energy Systems Inc. The authors are grateful to Professor J. Weitsman and Mr Don Erdman for furnishing the samples, and to C. H. Hsueh and R. A. Lowden for reviewing the manuscript.

References

1. P. J. HERRA-FRANCO and L. T. DRZAL *Composites* **23** (1991) 2.
2. A. A. WERESZCZAK, M. K. FERBER and R. A. LOWDEN, *Ceram. Eng. Sci. Proc.* **14**(10) (1993) 156.
3. D. L. CALDWELL and D. A. JARVIE, in "33rd International SAMPE Symposium", Anaheim, CA, 7–11 March 1988.
4. J. I. ELDRIDGE, "Desktop Fibre Push-out Apparatus", NASA TM-105341 (1991).
5. D. K. SHETTY, *J. Am. Ceram. Soc.* **71** (1988) C107.
6. R. J. KERANS and T. A. PARTHASARATHY, *ibid.* **74** (1991) 1585.
7. C. LIANG and J. W. HUTCHINSON, *Mech. Mater.* **14** (1993) 207.
8. C. H. HSUEH, *Mater. Sci. Eng.* **A154** (1992) 125.
9. K. T. FABER, S. H. ADVANI, J. K. LEE and J. T. TINN, *J. Am. Ceram. Soc.* **69** (1986) C208.
10. D. H. GRANDE, J. F. MANDELL and K. C. C. HONG, *J. Mater. Sci.* **23** (1988) 311.
11. A. E. GIANNAKOPOULOS, "Finite Element Simulation of Fiber Indentation Experiments with Coulomb Friction Interfaces", Department of Solid Mechanics, Royal Institute of Technology, Stockholm, Sweden (1989).
12. S. K. MITAL and C. C. CHAMIS, *JCTRER* **13** (1991) 14.
13. M. N. KALLAS, D. A. KOSS, H. T. HAHN and J. R. HELLMANN, *J. Mater. Sci.* **27** (1992) 3821.
14. D. B. MARSHALL, *Acta Metall. Mater.* **40** (1992) 427.
15. S-W. WANG and A. PARVIZI-MAJIDI, *Ceram. Eng. Sci. Proc.* **11** (1990) 1607.
16. S-W. WANG, A. KHAN, R. SANDS and A. K. VASUDEVAN, *J. Mater. Sci. Lett.* **11** (1992) 739.
17. T. J. MACKIN and F. W. ZOK, *J. Am. Ceram. Soc.* **75** (1992) 3169.
18. D. S. BEYERLE, S. M. SPEARING, F. W. ZOK and A. G. EVANS, *J. Am. Ceram. Soc.* **75** (1992) 2719.
19. A. W. PRYCE and P. A. SMITH, *Acta Metall. Mater.* **41** (1993) 1269.
20. I. M. DANIEL, G. ANASTASSOPOULOS and J. W. LEE, "Ceramic Matrix Fiber Composites Under Longitudinal Loading", *Compos. Sci. Technol.* **46** (1993) 105.
21. C. CHO, J. W. HOLMES and J. R. BARBER, *J. Am. Ceram. Soc.* **74** (1991) 2802.
22. D. B. MARSHALL and W. C. OLIVER, *J. Am. Ceram. Soc.* **70** (1987) 542.
23. C-H. HSUEH, M. K. FERBER and A. A. WERESZCZAK, *J. Mater. Sci.* **28** (1993) 2227.
24. C.-H. HSUEH, *J. Am. Ceram. Soc.* **76**(12) (1993) 3041.
25. P. S. STEIF and A. DOLLAR, *ibid.* **75** (1992) 1694.
26. A. DOLLAR and P. S. STEIF, *ibid.* **76** (1993) 897.
27. F. S. ACTON, "Numerical Methods that Work" (Harper and Row, New York, 1970).
28. T. A. PARTHASARATHY, P. D. JERO and R. J. KERANS, *Scripta. Metall. Mater.* **25** (1991) 2457.

Received 28 September 1993
and accepted 16 May 1994